

Probability distributions for measures of placental shape and morphology

J. S. Gill^a, M. P. Woods^a, C. M. Salafia^b, D. D. Vvedensky^a

^a*The Blackett Laboratory, Imperial College London, London SW7 2AZ, United Kingdom*

^b*Placental Analytics LLC, 93 Colonial Avenue, Larchmont, New York 10538*

Abstract

Goal. Weight at delivery is a standard cumulative measure of placental growth. But weight is a crude summary of other placental characteristics, such as the size and shape of the chorionic plate and the location of the umbilical cord insertion. Distributions of such measures across a cohort reveal information about the developmental history of the chorionic plate that is unavailable from an analysis based solely on the mean and standard deviation.

Methods & Materials. Various measures were determined from digitized images of chorionic plates obtained from the Pregnancy, Infection, and Nutrition Study, a prospective cohort study of preterm birth in central North Carolina between 2002 and 2004. The centroids (the geometric centers) and umbilical cord insertions were taken directly from the images. The chorionic plate outlines were obtained from an interpolation based on a Fourier series, while eccentricity (of the best-fit ellipse), skewness, and kurtosis were determined from a shape analysis using the method of moments. The distribution of each variable was compared against the normal, lognormal, and Lévy distributions.

Results. We found only a single measure (eccentricity) with a normal distribution. All other placental measures required lognormal or “heavy-tailed” distributions to account for moderate to extreme deviations from the mean, where relative likelihoods in the cohort far exceeded those of a normal distribution.

Conclusions. Normal and lognormal distributions result from the accumulated effects of a large number of independent additive (normal) or multiplicative (lognormal) events. Thus, while most placentas appear to develop by a series of small, regular, and independent steps, the presence of heavy-

tailed distributions suggests that many show shape features which are more consistent with a large number of correlated steps or fewer, but substantially larger, independent steps.

Keywords: placental measures, chorionic plate, shape, distributions

1. Introduction

The placenta is the interface across which all oxygen and nutrients are exchanged between mother and fetus. Understanding the development and function of the human placenta is crucial to gaining insight into the environment of the developing fetus, whose health is thought to be an important influence on childhood and lifelong health [1].

The placenta is conventionally thought to develop uniformly outward from the site of the umbilical cord insertion, leading to an approximately circular shape. However, while circular placentas are infrequently observed, recent work [2] has suggested that the “average” placental shape within a cohort is, in fact, close to circular, though there remains some debate on this issue [3, 4]. The ability of the chorionic late to extend laterally uniformly outward from the cord insertion is due, in part, to the suitability of the maternal uteroplacental environment. Any deficiencies in that environment can have adverse effects on placental and, by extension, fetal development. Consequently, the analysis of the deviations of mature placental chorionic surface shapes from “regularity” (circular, or otherwise) can provide information about the uterine environment and possibly provide indicators about the health of the child.

The structure of the mature placenta is geometrically complex. The umbilical cord is usually attached near the center of the placenta, but this is not always the case; eccentric, marginal and velamentous cords inserted onto the extraplacental membranes are not rare [5]. From the point of the cord insertion onto the chorionic plate, the fetal chorionic vascular system branches and spreads laterally across the chorionic plate. At later stages in the branching and extension of chorionic surface vessels, veins and arteries dive down into the placenta and continue branching to contribute to disk thickness. The chorionic surface outline of the delivered placenta is a culmination of lateral placental vascular growth.

A mature placenta can take many different shapes, from near-circular to multi-lobed to star-shaped. There is little or no explanation as to why such

variations of placental shapes exist, apart from “trophotropism” [6–8], an argument which says, in effect, that “the placenta grows where it can and does not grow where it cannot”. There is no data about whether shape variations are associated with particular complications or subsequent health problems. One of the main goals of the present study is to understand the genesis, development, and evolution of mature placental chorionic surface shape from the distributions of various measures of placental shape. The shape of a placental chorionic surface or, indeed, any two-dimensional object, can be characterized by area, perimeter, compactness (perimeter squared divided by area), eccentricity (of a bounding ellipse), elongation and rectangularity (of a bounding box), etc. In addition, the chorionic plate outline can be analyzed in terms of its “roughness” and “correlation”, both of which are standard measures used in the statistical analysis of rough surfaces [9]. The eccentricity and orientation of the best-fit ellipse, skewness, and kurtosis can be calculated from the lower-order moments of the chorionic plate [10, 11], and the distance between the umbilical cord insertion and the centroid, which provides an indication about how the placenta developed with respect to the umbilical cord, is extracted directly from the images. The roughness and correlation function are based on a Fourier representation of each chorionic plate outline.

Although an ideal placental shape is expected to be regular, if only to minimize the cost of maintaining its vascular network, deviations from regularity can be quite pronounced, as noted above, and are not uncommon. This indicates that the lateral growth of the placental chorionic surface is not typically a uniform process, but has an element of randomness in many, if not most pregnancies, that is, different regions of the placental chorionic surface may develop at different random rates. The potentially important corollary to this is that the “fetal programming” hypothesis may be germane to the majority of births, since few placentas are round with perfectly central cords. Various measures can and have been extracted from digitized images of placentas [12] and plotted as distributions, but an analysis of their distributions has yet to be reported. Our fundamental premise is that the form of these distributions can provide information about the statistical properties of these measures that encode the underlying developmental properties that led to these distributions. Attaining a better understanding of the timing of development of placental chorionic surface shape features, which may reflect early perturbations of placental vascular growth [2] may clarify how risk of the wide range of diseases that have been associated with gestational pathol-

ogy develops, or when in subsequent pregnancies of that mother surveillance might be expected to be useful in identification of recurrence, since there is a low but finite risk of recurrence after preeclampsia [13], preterm birth [14], fetal growth restriction [15], stillbirth [16], or even miscarriage [17, 18].

Placental growth has been shown to be empirically modeled by growth of a fractal by diffusion-limited aggregation [19]. From this basic observation, we can consider the notion of a random walk [20], where a “walker” takes small sequential steps to the left or right, each chosen randomly with equal probability. As the number of steps increases, the distribution of possible distances from the walker’s initial position approaches a normal distribution. An alternative version of a random walk is based on independent random *relative* increments which, as the number of steps increases, leads to a log-normal distribution [21]. Finally, a random walk with step sizes that decay as a power law for large step lengths is known as a “Lévy flight”. The likelihood of a large step is much greater than for a random walk, which has the effect of enhancing the rate of displacement compared to a random walk, and the resulting displacements follow the Lévy distribution [22].

2. Methods & Materials

2.1. *The Placental Cohort*

The data set for our analysis is obtained from the digital images of placentas collected from the Pregnancy, Infection, and Nutrition Study, a cohort study of women recruited at mid-pregnancy from an academic health center in central North Carolina. The study population and recruitment techniques are described in detail elsewhere [23]. Beginning in March 2002, all women recruited into this study were requested to consent to a detailed placental examination. As of October 1, 2004, 1159 women (94.6%) consented to such examination and 1014 (87.4%) had placentas collected and photographed for image analysis. Of these, 1008 (99%) were suitable for analysis.

Placental gross examinations, histology reviews, and image analyses were performed at EarlyPath Clinical and Research Diagnostics, a New York State-licensed histopathology facility under the direct supervision of Dr. Carolyn Salafia. The institutional review board from the University of North Carolina at Chapel Hill approved this protocol. The fetal surface of each placenta was wiped dry and placed on a clean surface, after which the extraplacental membranes and umbilical cord were trimmed from the placenta.

The fetal surface was photographed with the laboratory identification number together with 3 cm of a plastic ruler in the field of view using a standard high-resolution digital camera with a minimum image size of 2.3 megapixels. A trained observer captured the (x, y) coordinates that marked the site of the umbilical cord insertion and a series of such points along the perimeter of the fetal surface. The perimeter coordinates were captured at intervals no greater than 1 cm, with additional coordinates if it appeared essential to accurately capturing the shape of the fetal surface.

2.2. Measures of Chorionic Plate Shape and Morphology

A Fourier series (Appendix A) is used to interpolate between the discrete points captured along the perimeter of the chorionic plate (Sec. 2.1), resulting in a smooth outline. A Fourier series is a sum of trigonometric functions (sines and cosines) whose coefficients measure the deviation of the outline from circularity. If only small deviations are present, then the first few terms in this series are sufficient. But more terms are required to capture an outline that has rapidly-varying features, such as lobes and protrusions. This interpolation is used to calculate moments of the region surrounded by the outline (Appendix B). With increasing order, these moments provide successively more detailed information about the shape and morphology of the chorionic plate. Both the Fourier coefficients of the outline and the moments of the region surrounded by the outline are used to calculate measures of the shape and morphology of the chorionic plate. Table 1 summarizes the measures and their formulas.

The area bounded by the chorionic outline provides a cumulative measure of the development of the placenta at delivery. No information is provided about the shape or morphology of the chorionic plate – this is contained in higher moments. The skewness measures the asymmetry with respect to the mean of projections of the image onto the x - and y -axes, viewed as distributions. Similarly, the kurtosis measures the peakedness or flatness of these projections relative to that of a normal distribution, whose kurtosis has the value 3. Thus, a positive (resp., negative) kurtosis means that the distribution is more (resp., less) peaked than a normal distribution. Each chorionic plate has also been represented by an ellipse, whose eccentricity and orientation are determined by the zeroth and first moments.

The chorionic plate outline provides complementary information to the moment analysis. The two measures we use are the roughness and the correlation function. The roughness, defined in (A.5), is an average over the

Table 1: Measures of the chorionic plate that are calculated in this paper. Against the name of each measure is its symbol, definition, and a formula expressed in terms of moments μ_{ij} of the region bounded by the chorionic plate outline (Appendix B) or the Fourier coefficients a_n and b_n of the outline (Appendix A). The fundamental mathematical definitions of these measures, from which the formulas in this table are derived, are given in Appendices A and B.

Name	Symbol	Definition	Formula
Area	A	Area within chorionic plate outline	μ_{00}
Centroid	(x_c, y_c)	Geometric center of area within chorionic plate outline	$\left(\frac{\mu_{10}}{\mu_{00}}, \frac{\mu_{01}}{\mu_{00}}\right)$
Eccentricity	e	Eccentricity of bounding ellipse	$\sqrt{1 - \frac{b^2}{a^2}}$
Skewness	(S_x, S_y)	Asymmetry of image projections onto x - and y -axes	$\left(\frac{\mu_{30}}{\mu_{20}^{3/2}}, \frac{\mu_{03}}{\mu_{02}^{3/2}}\right)$
Kurtosis	(K_x, K_y)	Peakedness relative to normal distribution of image projections onto x - and y -axes	$\left(\frac{\mu_{40}}{\mu_{20}^3} - 3, \frac{\mu_{04}}{\mu_{02}^3} - 3\right)$
Roughness	W	Standard deviation of chorionic outline from the average radius	$\left[\frac{1}{2} \sum_{n=1}^N (a_n^2 + b_n^2)\right]^{1/2}$
Correlation Function	$C(s)$	Standard deviation of chorionic outline as a function of separation	$\left[2 \sum_{n=1}^N (a_n^2 + b_n^2) \sin^2\left(\frac{\pi sn}{L}\right)\right]^{1/2}$

chorionic plate outline of root-mean-squared deviations from an average radius. Thus, roughness measures the “width” of the deviations of the outline from a circle. A small roughness indicates a narrow width, which corresponds

to an approximately circular outline, while a large width results from larger deviations from circularity, such as those of lobed or star-shaped outlines.

A related measure of the irregularity of the outline is the correlation function, defined in (A.7) as the standard deviation of differences between all pairs of radii on the chorionic plate outline at a fixed separation. Whereas the roughness measures the deviation from circularity by summing individual points along the outline, yielding a *number*, the correlation function involves differences between radii at a fixed separations along the outline, which is expressed as a *function* of this separation. Thus, the correlation function is measure of roughness that is spatially resolved along the chorionic plate outline. In this paper, however, we will not discuss the spatial dependence of the correlation function, but focus on its average properties.

2.3. Probability Distributions

When calculated for all of the placentas in our cohort, the measures compiled in Table 1 yield ranges of values that can be represented as distributions, that is, the relative frequencies of occurrences of the outcomes of the measures. These distributions embody information about the developmental characteristics of placentas, which can be identified by comparing them with distributions that are associated with particular types of processes. The distribution functions that we use in this paper are summarized below, with details provided in Appendix C.

The most common probability distribution is the Gaussian, or **normal**, distribution. The probability density of this distribution is completely characterized by its mean μ and standard deviation σ . Normal distributions are so common because of the central limit theorem, which states that such distributions are the cumulative result of a large number of *additive* random events [20]. A related distribution is the **lognormal**, which is the probability of a variable whose *logarithm* is normally distributed [21]. The lognormal is a skewed distribution, which occurs when averages are low, variances comparatively large, and values of the quantity being measured cannot be negative. This distribution is the cumulative result of a large number of *multiplicative* random events.

A distribution that is qualitatively different from the normal and log-normal distributions is the symmetric **Lévy** distribution [22]. The main distinguishing characteristic of Lévy distributions is that the probability of extreme variations decays like a *power* of that variation, as indicated in (C.7). Hence, the occurrence of such variations is far more likely than for a normal

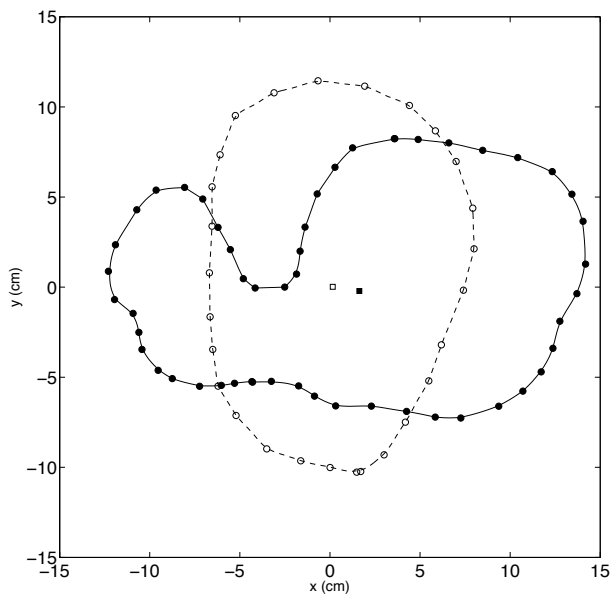


Figure 1: Two examples of interpolations of chorionic plate outlines that have been determined by the method described in Appendix A. The origin of the data points for each outline has been shifted to its centroid. The open circles mark the original data points and the broken curve shows the interpolation for an outline with a single-valued radius function. The corresponding umbilical cord insertion is indicated by the interior open circle. The closed circles mark the original data points and the solid curve shows the interpolation for an outline with a multi-valued radius function. The corresponding umbilical cord insertion is indicated by the interior closed circle.

distribution, which decays *exponentially*. For this reason, Lévy distributions are called “heavy tailed.” Lévy distributions arise from additive random events which may involve quite large changes. In contrast, the events that result in the normal and lognormal distributions are comparatively small.

3. Results

3.1. Interpolation of Chorionic Plate Outlines

Figure 1 shows typical fits to the data points of chorionic plate outlines obtained with the method described in Appendix A. Two types of outlines are shown: one with a single-valued and one with a multi-valued radius. A single-valued radius means that a line emanating from the centroid intersects every point on the perimeter only once, while a multi-valued radius function may intersect the perimeter more than once. In the latter case, the perimeter

folds back on itself, and the corresponding chorionic plate has lobes or some other irregular shape. Note the irregular spacing of the points along the perimeter, as described in Sec. 2.1. The outline with the single-valued radius has a regular shape, so relatively few data points are needed. However, the outline with the multi-valued radius has intervals where more points are needed to describe regions of greater curvature, which can occur for a small protrusion or, as in this case, a large morphological entity such as a lobe. This is reflected in the number of terms that must be included in the Fourier series to produce an accurate interpolation. The series for the outline with the single-valued radius required fewer terms than that for the outline with the multi-valued radius because regions of larger curvature mean that more rapidly varying trigonometric functions must be included in the interpolation.

3.2. Chorionic Plate Area

The distribution of areas A bounded by the outlines of the chorionic plates are shown as a histogram in Fig. 2. These histograms were constructed by first defining normalized areas as the original areas A divided by the average area A_{av} of the cohort. These data points are grouped into contiguous “bins” of width 0.1, a choice dictated by the balance between the inherent statistical fluctuations in such a limited sample against the smoothness of the resulting relative frequency profile. Choosing a width of 0.05 produced a somewhat noisier distribution but did not substantially alter any of the fits. The relative frequencies f are obtained by dividing the fraction of the total number of data points within each bin by the bin width, so the shaded area in the histogram in Fig. 2 is equal to 1. This way of plotting histograms, which eliminates the units of the quantities being plotted, allows distributions of different measures to be compared directly, as well as providing the conceptual convenience of having the mean at 1.

Superimposed on the area histogram are the normal (a) and lognormal (b) distributions with mean and standard deviation determined from the data, in the latter case using (C.3) and (C.4), and an optimized fit to a Lévy distribution (c), which yielded the parameters $\alpha = 1.62 \pm 0.02$ and $\gamma = 0.046 \pm 0.04$ in (C.5). This fit was obtained by the least squares method, wherein a Lévy distribution was calculated at the center of each bin, and the sum of the squares of the differences between these values and those of the bins was minimized by varying α and γ . Figures 2(b,d,f) show the same distributions plotted on a logarithmic scale for the frequencies (but maintaining the same linear scale for the areas). Such plots are used to accentuate the

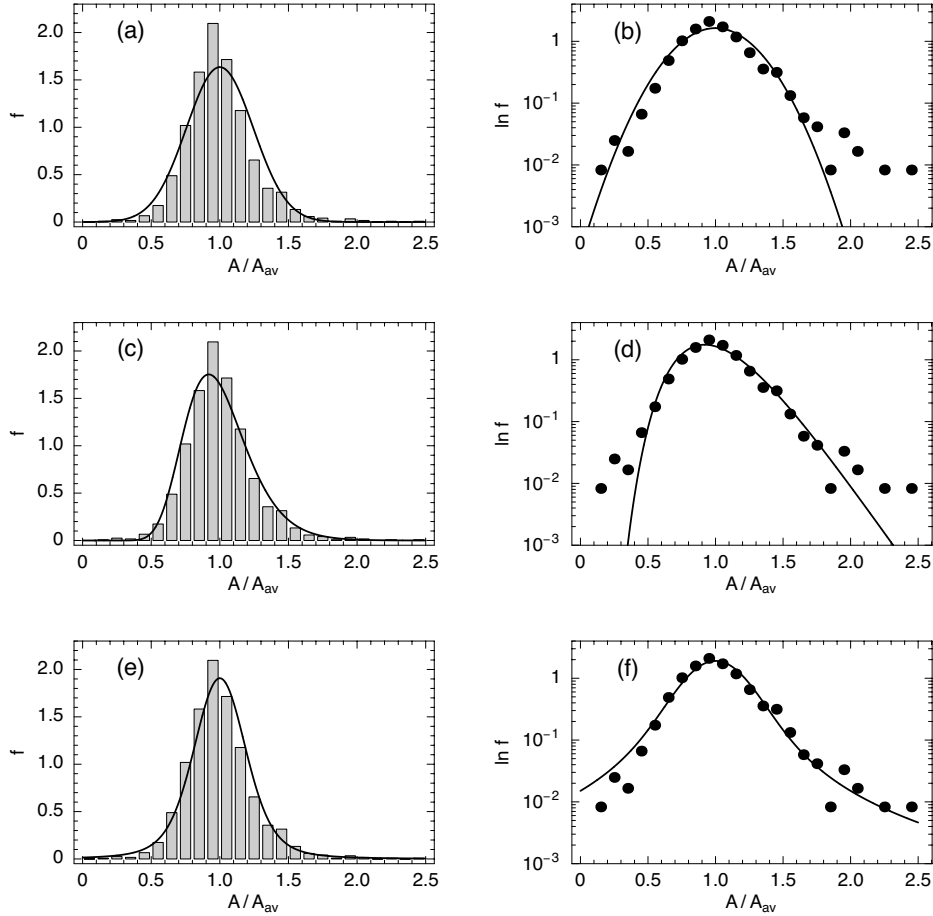


Figure 2: Histogram of chorionic plate areas shown as the relative frequencies of bins of normalized areas. These are compared with (a,b) the normal distribution, (c,d) the lognormal distribution, and (e,f) an optimized Lévy distribution, each of which is shown by a solid curve. The histogram and distributions are plotted on a logarithmic scale for the relative frequencies, indicated as points, in (b,d,f).

extreme variations of data (the “tails” of the relative frequencies) to assess how various distributions account for this regime. Note that, according to (C.7), the fit in Fig. 2(c), yields a probability for large deviations from the mean decreases as $(A/A_{av})^{-2.62}$.

3.3. Perimeter Roughness and Correlation Function

Measures of the chorionic plate outline that provide information about shape are the roughness of the perimeter(A.5) and the integrated correlation

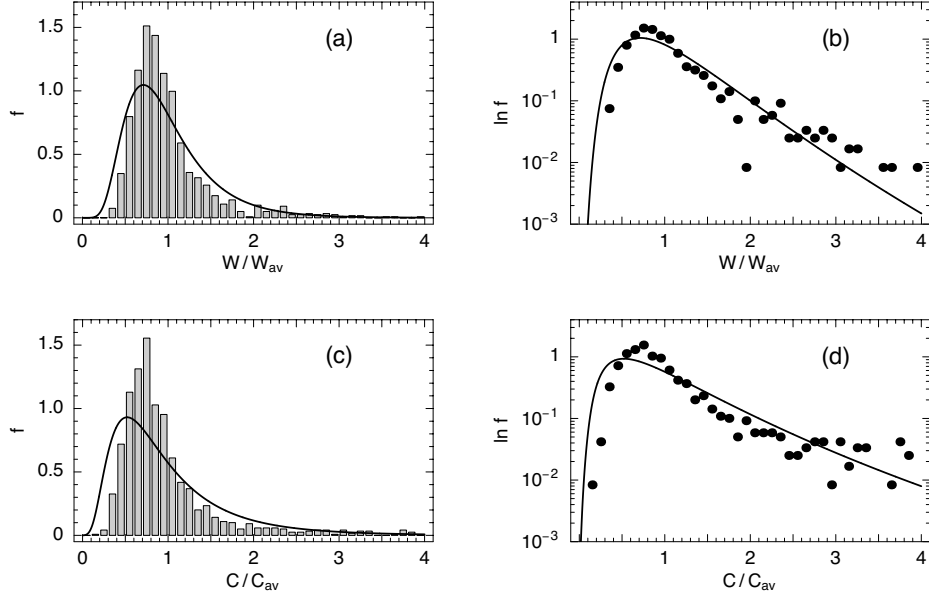


Figure 3: Histograms of the roughness (a,b) and the integrated correlation function in (A.9) (c,d). Linear plots are shown in (a) and (c) and the corresponding plots with a logarithmic frequency scale in (b) and (d) with the frequencies associated with each bin indicated by points. Each of the histograms is compared with a lognormal distribution, which is indicated by the solid curve.

function (A.9). Figure 3(a,c) shows the histograms of these quantities, with each normalized as in Fig. 2, i.e. each measure is divided by its average over the cohort and the frequencies are defined such that the sum of the shaded regions is equal to 1. The bin width for each histogram was again taken as 0.1. Plotted with each histogram is a lognormal distribution whose mean and standard deviation were determined from the data by using (C.3) and (C.4). Figure 3(b,d) shows the histograms and corresponding lognormal distributions plotted on a logarithmic scale for the frequencies. The tails of these distributions extend to much larger values than the area distributions in Fig. 2, so the semi-logarithmic plots provide correspondingly more information about the distribution. These histograms are significantly skewed, so only the lognormal distribution is appropriate, as both the normal and Lévy distributions are symmetric.

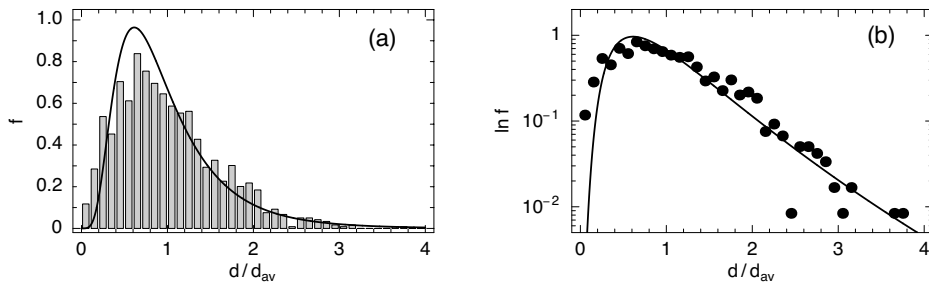


Figure 4: (a) Histogram of the distances between the centroid and the umbilical cord insertion compared with the lognormal distribution. (b) Semi-logarithmic plot of the histogram and distributions in (a), with the bin frequencies represented by points.

3.4. Distance between the Centroid and the Umbilical Cord Insertion

As the placenta grows outwards from a central point, the position of the umbilical cord insertion relative to the centroid of the placenta, which is a measure of the centrality of this point, provides information about the isotropy of placental development. If the umbilical cord insertion is close to the centroid, then the placenta has, on average, grown outwards more symmetrically than if the cord insertion is displaced appreciably from the centroid. This does not imply that the chorionic plate is circular in this case, just that lateral growth was not skewed in any direction. The histogram of the distances between the centroid and the umbilical cord insertion is shown in Fig. 4, plotted with the distances divided by their average, with frequencies that sum to 1. The data have been grouped into bins of width 0.1. Superimposed on the histograms are the lognormal distribution whose mean and standard deviation are determined from the data by using (C.3) and (C.4). Note that, in common with the histograms in Fig. 3, the histogram of the distances is highly skewed, with a long tail, so only the lognormal distribution is appropriate.

3.5. Placental Shape

The moment expansion method described in Appendix B has been used to calculate the best-fit ellipse for the chorionic plate of each placenta in the cohort. This includes the semi-major and semi-minor axes and the orientation angle. Figure 5 shows a selection of placentas together with their best-fit ellipses. Most apparent from this figure is that some outlines fit their ellipse quite well. These correspond to chorionic plates with regular shapes. For chorionic plates with irregular shapes that have pronounced lobes and

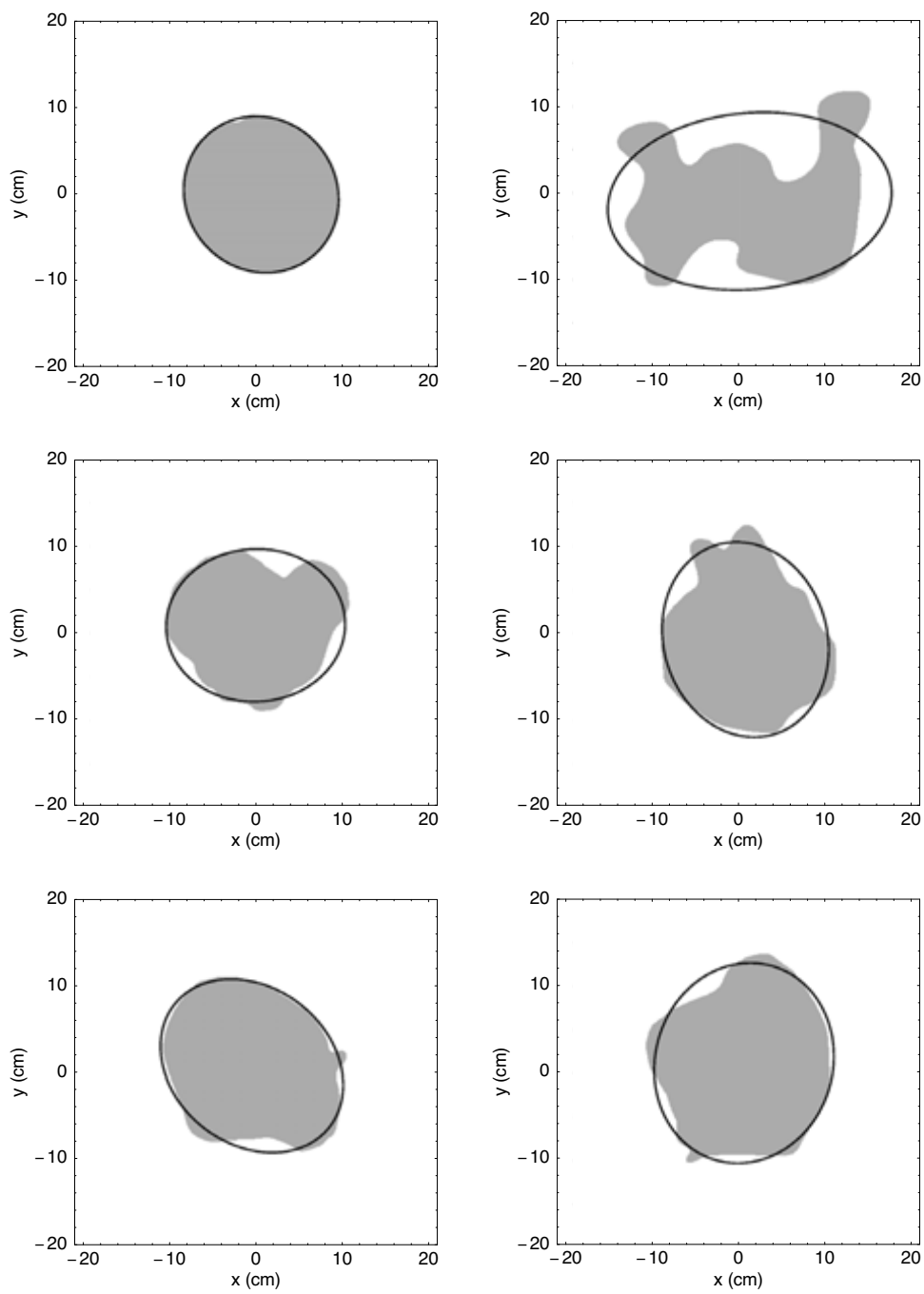


Figure 5: Chorionic plates (shown shaded) and best-fit ellipses (solid curves) for a selection of placentas from our cohort.

other protrusions, the ellipse does not provide as good a fit. As expected from the discussion in Appendix B, such placentas have appreciable higher-order moments to account for their irregularities. In such cases, quantities derived from higher-order moments, such as skewness (third-order) and kurtosis (fourth-order) provide significant additional information about placental shape. The extent to which the ellipse accounts for the shape of the chorionic plate can also be used to estimate the roughness. Any region of the chorionic outline that lies within the ellipse or crosses its boundary contributes to the roughness, as is apparent from the definition in (A.5).

Figure 6(a) shows the histogram of the eccentricities with a superimposed normal distribution that has the same mean and variance. The bin sizes were 0.04 for the eccentricity and kurtosis and 0.05 for the skewness. Figure 6(a,c,e) shows comparisons of these histograms with normal distributions that have the same mean and standard deviation as the data, while Fig. 6(b,d,f) shows comparisons with optimized Lévy distributions using the procedure described in Sec. 3.2. The optimized parameters are $\alpha = 2$ and $\gamma = 0.012$ for the eccentricity, $\alpha = 1.6$ and $\gamma = 0.009$ for the skewness, and $\alpha = 1.75$ and $\gamma = 0.0036$ for the kurtosis, with the same error bars as in Sec. 3.2. For the skewness and kurtosis, the fits were carried out for the averages over the x - and y -projections of each quantity.

4. Discussion

There are large variations in the characteristics of mature placental shapes. How do these variations arise? The uterine environment plays a part, for example, in cases where “trophotropism” suggests that the placenta can differentially grow, effectively migrating to a more suitable location in the uterus. However, there may also be manifestations of randomness within placental growth. The chorionic plate outline of the mature placenta reflects, in essence, a summary of the effects of all factors that can impact the lateral expansion of the chorionic surface. Identifying whether a placental measure follows one of the distributions in Appendix C or another distribution is important for assessing the statistical properties of lateral growth or the processes underlying growth. The results we described in the preceding section are summarized in Table 2.

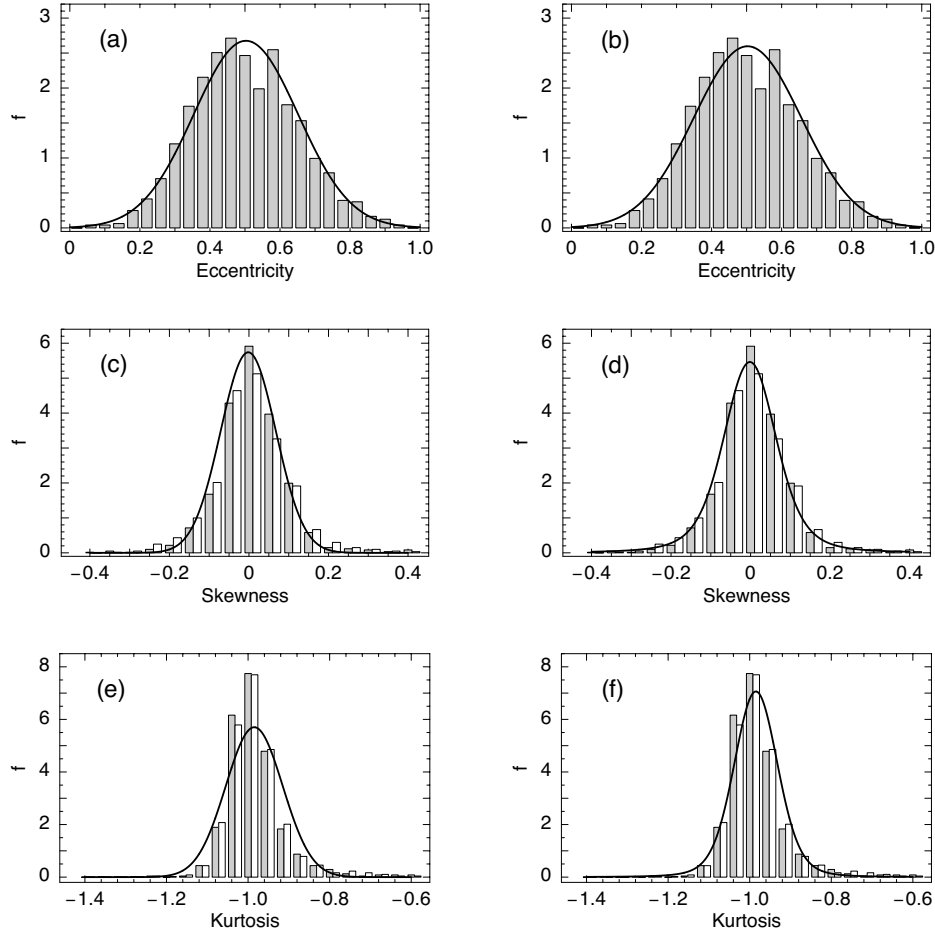


Figure 6: Histograms of the eccentricities of the best-fit ellipses compared with (a) a normal and (b) an optimized Lévy distribution. Histograms of the skewness of the chorionic plate, projected onto the x - and y -axes (shown as shaded and unshaded bins, respectively) compared with the (c) normal and (d) an optimized Lévy distribution. Histograms of the kurtosis of the chorionic plate, projected onto the x - and y -axes (shown as shaded and unshaded bins, respectively) compared with the (e) normal and (f) an optimized Lévy distribution. The fits in (c)–(f) were obtained by averaging over the x - and y -projections of each quantity.

4.1. Chorionic Plate Area

The Gaussian and lognormal distributions provide good accounts of the gross shape of the histogram of chorionic plate areas, but underestimate the peak near the mean [Fig. 2(a)]. The larger positive deviations from the mean

Table 2: Summary of best-fit distributions for the measures in Table 1, as well as the distance between the centroid and the umbilical cord insertion.

Measure	Best Fit	Comments
Area	Lévy	Normal distribution for small values, Lévy distribution for moderate to large values
Roughness	lognormal	power law (“heavy”) tail
Correlation Function	lognormal	power law (“heavy”) tail
Centroid–Umbilical Cord Distance	lognormal	poor fit near peak of histogram
Eccentricity	normal	optimized Lévy distribution also yields normal distribution
Skewness	Lévy	average over x - and y - directions
Kurtosis	Lévy	average over x - and y - directions

of the area are better described by the lognormal distribution, but the Lévy distribution provides a discernibly better overall fit to the entire histogram than either the normal or lognormal distributions [Fig. 2(c)]. In particular, the Lévy distribution gives a much better account of the peak near the mean and at large positive deviations from the mean, where the decay is much slower than for the normal distribution. This can be seen directly in Fig. 2(b,d), where we plot the logarithm of the frequencies in Figs. 2(a,c) against the normalized area. In this coordinate system, the normal distribution appears as an inverted parabola, as follows from (C.1). Figure 2(b,d) clearly shows that the lognormal distribution provides a good fit for moderate

positive deviations from the mean, but that the Lévy distribution provides a much better fit at all large positive deviations from the mean. The normal distribution, however, provides a better description of the data at values below the mean.

To appreciate the consequences of the better fit provided by the Lévy distribution, we return to the notion of a random walk [20], where a “walker” takes small sequential steps to the left or right, each chosen randomly with equal probability. As previously noted, as the number of steps increases, the distribution of possible distances from the walkers initial position approaches a normal distribution. Lévy distributions arise from random walks with step sizes chosen from a distribution for which step sizes decay as a power law for large step lengths. Hence, the likelihood of a large step is much greater than for a random walk. This has the effect of enhancing the rate of displacement compared to a random walk. The fits in Fig. 2 thereby suggest that placentas whose chorionic plate area is much smaller than the mean, which follow a normal distribution, developed by a series of small independent random steps. Placentas with a chorionic area that is much larger than the mean, however, developed by large steps, or a series of smaller correlated steps. In either case, the growth of placentas with a large chorionic area is manifestly inconsistent with normal behavior.

4.2. Perimeter Roughness and Correlation Function

The skewed histograms in Fig. 3 mean that symmetric distributions are not appropriate, so we have focused on the lognormal distribution. This distribution provides a reasonable fit to the data, though there are evident discrepancies, especially for small values of the correlation function. However, as the semi-logarithmic plots in Fig. 3(b,d,f) show, while the lognormal distribution accurately accounts for moderate positive deviations from the mean, extreme deviations (the tails) show systematic differences from this distribution.

An analysis of this regime is carried out in Fig. ??, where we show log-log plots of the data in Figs. 2(a,c,e) together with a linear fit to the tails of each distribution. Bearing in mind that there are fewer placentas for extreme values, so the scatter in the data is correspondingly greater than for smaller values, the linear fits provide an acceptable account of these tails. The significance of this becomes apparent when we refer to the discussion in Appendix C and, in particular, the power law behavior of the tails of the Lévy distribution in (C.6). The linear fits in Fig. 7 show that the tails of

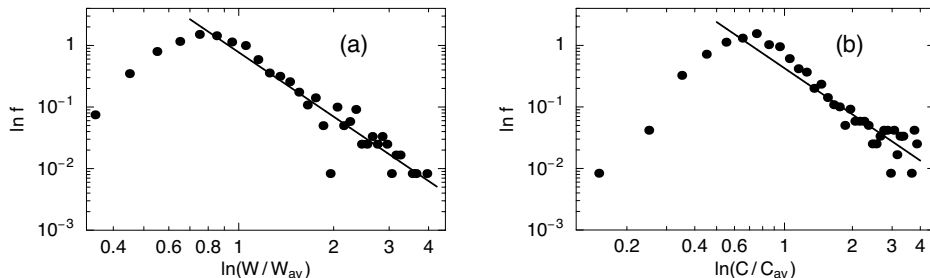


Figure 7: Log-log plots of the histograms in Fig. 3(a,c), with the bin frequencies represented as dots. The lines in each panel represent an optimized linear fit to the tails of the distributions, with slopes of -3.47 and -2.49 , respectively. The quality of these fits suggest that the tails of the corresponding distributions have a power law decay, as in (C.6).

these histograms are indeed consistent with a power law decay. Although this is indicative of the wild fluctuations associated with Lévy distributions, we have not been able to fit a Lévy distribution to the entire range of the data. Nevertheless, the analysis in Fig. 7 is very suggestive. But we conclude this discussion with a word of caution. Linear fits to log-log plots typically rely on several decades (i.e. powers of ten on a log-log plot) of data to enable a firm conclusion to be drawn about the existence of power law tails. Our analysis is based on less than half a decade, which is the nature of the measures we are using, so our conclusions must be tempered accordingly.

4.3. Distance between the Centroid and the Umbilical Cord Insertion

The lognormal distribution in Fig. 4 provides a good account of the profile of the histogram of distances between the centroid and the umbilical cord insertion – only the main peak of the histogram is overestimated by approximately 10%. Even more significant is the fit in Fig. 6(b), which shows that the lognormal distribution provides an excellent account of the tail of the histogram. Hence, we conclude that the distribution associated with this quantity, when measured in mature placentas across a cohort, is the cumulative result of small multiplicative random steps. This, in turn, leads to two further considerations. Consider first the fact that a vasculogenic zone is already evident at the 5th week of development [24]. Thus, in the early stages of development, we expect that the centroid of the developing chorionic plate and umbilical cord insertion are strongly correlated. However, as further development occurs, random factors diminish this corre-

lation, eventually producing the uncorrelated behavior seen in Fig. 4. Why is the distribution lognormal, rather than normal? Chemical reactions and, by extension, biochemical reactions, are inherently multiplicative processes [21] because concentrations of particular species must be simultaneously present at a specific location for development to occur. The amount of each quantity, which varies across the placenta, determines the extent to which development occurs. The comparisons in Fig. 4 suggests that these spatial variations are random.

4.4. Placental Shape

The most striking result in Fig. 6 is how well the normal distribution accounts for the eccentricities of the best-fit ellipses across the cohort. This is confirmed by the optimized Lévy distribution, which has ($\alpha = 2$) and a standard deviation of $\sqrt{2\gamma} = 0.0155$, the latter comparing well with the value $\sigma = 0.0149$ obtained directly from the data. Hence, the eccentricity may be regarded as being normally distributed. The shape of the skewness is also described moderately well by a normal distribution, though the large deviations from the mean are better accounted for by the Lévy distribution. For the kurtosis, the normal distribution accounts for the width of the distribution, but underestimates the height of the peak near the mean and, of course, does not account for the occurrence of large deviations from the mean. Here, the Lévy distribution provides the superior description.

5. Summary

Placental weight is a standard measure of placental development and is often used as a primary indicator of fetal health. But weight is just one way that factors affect the developmental history of a placenta. Other measures have been presented before [12] and are revisited here in light of their distributions. Working from interpolations between data points obtained from digitized images of the cohort described in Ref. [23], we have calculated several measures of chorionic plate morphology, including its area, the roughness and correlation function of the outline, the distance between the centroid and the umbilical cord insertion, and several shape parameters.

Our focus here is determining the extent to which the distributions of placental measures are described by normal or lognormal distributions, in other words, the extent to which the fluctuations of these measures result from the sum or product, respectively, of relatively *independent* factors. In

fact, we found that normal distributions provide an accurate account only of the distribution of the eccentricities of the best-fit ellipses. Taken together, the results presented here demonstrate how an analysis of a cohort can reveal fundamental aspects in the development of placentas. The deviations from normal or log-normal behavior, in particular, provide the most direct indication of the presence of correlations in the development of the placenta. Large deviations from mean behavior are not simply the result of mild independent fluctuations, as normal or lognormal distributions would imply, but embody the wild fluctuations that lead to power law decay. While we have focused entirely on geometric and morphological features in this paper, other characteristics of the chorionic plate would also benefit from our analysis, especially those which take account of vasculature. Such studies are in progress and will be reported in a future publication.

Appendix A. Fourier Series for the Chorionic Plate Outline

The chorionic plate outline is represented by a set of points with coordinates (x_k, y_k) , for $k = 1, \dots, N$ obtained from the digitized images (Sec. 2.1). To eliminate any bias in the data, we first calculate the coordinates (x_c, y_c) of the centroid by taking the average of each perimeter coordinate:

$$x_c = \frac{1}{N} \sum_{k=1}^N x_k, \quad y_c = \frac{1}{N} \sum_{k=1}^N y_k. \quad (\text{A.1})$$

The centroid is taken as the origin of coordinates for the points along the chorionic outline. The radius r is specified in terms of the length s along the perimeter, which has length L . The Fourier series for $r(s)$ is

$$r(s) = r_{\text{av}} + \sum_{n=1}^N \left[a_n \cos\left(\frac{2\pi s n}{L}\right) + b_n \sin\left(\frac{2\pi s n}{L}\right) \right], \quad (\text{A.2})$$

where the Fourier coefficients are

$$a_n = \frac{2}{L} \sum_{k=1}^N r_k \cos\left(\frac{2\pi s_k n}{L}\right), \quad (\text{A.3})$$

$$b_n = \frac{2}{L} \sum_{k=1}^N r_k \sin\left(\frac{2\pi s_k n}{L}\right), \quad (\text{A.4})$$

in which r_k is the radius of the k th data point at a distance s_k along the perimeter. The corresponding series for the coordinates $(x(s), y(s))$ of the perimeter are of the same form as (A.2), but with x_k and y_k in turn replacing r_k in (A.3) and (A.4).

The interpolation of the chorionic plate outline can be used to calculate several measures associated with the deviations of this outline from circularity. The roughness W of this outline is defined as the root-mean-squared deviations from its average radius r_{av} :

$$W = \left\{ \frac{1}{L} \int_0^L [r(s) - r_{\text{av}}]^2 ds \right\}^{1/2}, \quad (\text{A.5})$$

in which $r(s)$ is the distance from the centroid to the chorionic plate outline at a point s along the outline and L is the length of the outline. The roughness

is expressed in terms of the coefficients in (A.3) and (A.4) as

$$W = \left[\frac{1}{2} \sum_{n=1}^{\infty} (a_n^2 + b_n^2) \right]^{1/2}. \quad (\text{A.6})$$

The correlation function $C(s)$, defined as

$$C(s) = \left\{ \frac{1}{L} \int_0^L [r(s+t) - r(t)]^2 dt \right\}^{1/2}, \quad (\text{A.7})$$

is the standard deviation of pairs of radii on the chorionic plate outline as a function of their separation, is expressed in terms of the coefficients in (A.3) and (A.4) as

$$C(s) = \left[2 \sum_{n=1}^{\infty} (a_n^2 + b_n^2) \sin^2 \left(\frac{\pi sn}{L} \right) \right]^{1/2}. \quad (\text{A.8})$$

The relation between the correlation function and the roughness can be obtained directly from (A.6) and (A.8):

$$\int_0^L C^2(s) ds = L \sum_{n=1}^N (a_n^2 + b_n^2) = 2LW^2, \quad (\text{A.9})$$

so the correlation function corresponds to a roughness that is spatially resolved along the chorionic plate outline.

Appendix B. Moments of Chorionic Plate Shape

An alternative to the contour-based analysis of chorionic plate shape using the Fourier series in Appendix A is the area-based approach of moments. We define a function $f(x, y)$ that takes the value 1 within the chorionic plate area and the value 0 outside this area. The (p, q) th moment $\mu_{p,q}$ of the enclosed area is defined as

$$\mu_{p,q} = \iint x^p y^q f(x, y) dx dy, \quad (\text{B.1})$$

where $p, q = 0, 1, 2, \dots$. If all of the moments are calculated, then the original shape can be restored. In practice, only lower-order moments, for which $p + q \leq 4$ are typically used.

The zeroth-order moment $\mu_{0,0}$ determines the area A of the chorionic plate,

$$A = \mu_{0,0} = \iint f(x, y) dx dy, \quad (\text{B.2})$$

and the coordinates (x_c, y_c) of the centroid are expressed in terms of $\mu_{0,0}$ the first-order moments $\mu_{1,0}$ and $\mu_{0,1}$ as

$$x_c = \frac{1}{A} \iint x f(x, y) dx dy = \frac{\mu_{1,0}}{\mu_{0,0}}, \quad (\text{B.3})$$

$$y_c = \frac{1}{A} \iint y f(x, y) dx dy = \frac{\mu_{0,1}}{\mu_{0,0}}. \quad (\text{B.4})$$

The zeroth- and second-order moments determine the best-fit ellipse.

This ellipse is centered at the centroid of the chorionic plate and its semi-major and semi-minor axes a and b , respectively, are the perpendicular lines that pass through the centroid for which the second-order central moments about these lines are maximum and minimum, respectively. The semi-major and semi-minor axes are given by [10]

$$a = \sqrt{2} \left\{ \frac{\mu_{2,0} + \mu_{0,2} + [(\mu_{2,0} - \mu_{0,2})^2 + 4\mu_{1,1}^2]^{1/2}}{\mu_{0,0}} \right\}^{1/2}, \quad (\text{B.5})$$

$$b = \sqrt{2} \left\{ \frac{\mu_{2,0} + \mu_{0,2} - [(\mu_{2,0} - \mu_{0,2})^2 + 4\mu_{1,1}^2]^{1/2}}{\mu_{0,0}} \right\}^{1/2}, \quad (\text{B.6})$$

where the tilt angle ϕ of the ellipse, measured counterclockwise with respect to the original coordinate axes, is [10]

$$\phi = \frac{1}{2} \tan^{-1} \left(\frac{2\mu_{1,1}}{\mu_{2,0} - \mu_{0,2}} \right). \quad (\text{B.7})$$

The convention is that ϕ is the angle between the x -axis and the semi-major axis, where, by definition, $a \geq b$. The eccentricity e of the best-fit ellipse is given by the usual formula:

$$e = \sqrt{1 - \frac{b^2}{a^2}}. \quad (\text{B.8})$$

Higher-order moments include quantities such as skewness and kurtosis of x and y projections of the placental shape (for example, the x -projection is the image obtained by summing over all pixels in the x -direction). Expressions for these quantities are compiled in Table 1.

Appendix C. Probability Density Functions

The probability density function $p(x)$ of a continuous random variable represents the relative likelihood that the random variable occurs at a given point x . The probability density function is nonnegative, and its integral over all possible values of x is equal to one. The probability density of the normal distribution is

$$p_1(x; \mu, \sigma) = \frac{1}{\sqrt{2\pi}\sigma} \exp\left[-\frac{(x - \mu)^2}{2\sigma^2}\right], \quad (\text{C.1})$$

in which μ is the mean σ the standard deviation. The corresponding quantity for the lognormal distribution is

$$p_2(x; \mu, \sigma) = \frac{1}{x\sqrt{2\pi}\sigma} \exp\left[-\frac{(\ln x - \mu)^2}{2\sigma^2}\right]. \quad (\text{C.2})$$

where μ is the mean and σ the standard deviation for $\ln x$. These are related to the mean μ' and variance σ'^2 of a random variable that is log-normally distributed by

$$\mu = \ln(\mu') - \frac{1}{2} \ln\left(1 + \frac{\sigma'^2}{\mu'^2}\right), \quad (\text{C.3})$$

$$\sigma^2 = \ln\left(1 + \frac{\sigma'^2}{\mu'^2}\right). \quad (\text{C.4})$$

The probability density function of the Lévy distribution

$$p_3(x; \alpha, \gamma) = \frac{1}{\pi} \int_0^\infty e^{-\gamma k^\alpha} \cos(kx) dk, \quad (\text{C.5})$$

where $0 < \alpha \leq 2$ and $\gamma > 0$ is a width parameter. The Lévy distribution is known in closed form only for $\alpha = 1$ and $\alpha = 2$, with the latter yielding the normal distribution in the form

$$p_3(x; 2, \gamma) = \frac{1}{\sqrt{4\pi\gamma}} \exp\left(-\frac{x^2}{4\gamma}\right), \quad (\text{C.6})$$

which is a normal distribution with $\mu = 0$ and $\sigma^2 = 2\gamma$. In all other cases the Lévy distribution must be evaluated numerically.

One of the most important characteristics of Lévy distributions is that the probability density of extreme variations of a random variable follows a power law:

$$p_3(x; \alpha, \gamma) \rightarrow |x|^{-\alpha-1} \quad \text{as} \quad |x| \rightarrow \infty. \quad (\text{C.7})$$

References

- [1] Barker DJ. Fetal origins of coronary heart disease. *British Medical Journal* **311**: 171–4 (1995).
- [2] Salafia CM, Yampolsky M, Misra DP, Shlakhter O, Haas D, Eucker B, Thorp J. Placental surface shape, function, and effects of maternal and fetal vascular pathology. *Placenta* **31**(11): 958–62 (2010).
- [3] Pathak S, Hook E, Hackett G, Murdoch E, Sebire NJ, Jessop F, Lees C. Cord coiling, umbilical cord insertion and placental shape in an unselected cohort delivering at term: Relationship with common obstetric outcomes. *Placenta* **31**(11): 963–968 (2010).
- [4] Nelson DM, Burton GJ. Does a picture of the human placenta predict the future? *Placenta* **31**(11): 943 (2010).
- [5] Benirschke K, Kaufmann P, Baergen RN. *Anatomy and Pathology of the Umbilical Cord*. 5th edition. (Springer, New York, 2006), p. 403, Table 12.2.
- [6] Ramos-Arroyo MA, Ulbright TM, Yu PL, Christian JC. Twin study: Relationship between birth weight, zygosity, placentation, and pathologic placental changes. *Acta Genet Med Gemellol (Roma)* **37**(3-4): 299–38 (1988).
- [7] Cunningham FG, MacDonald P, Gant N, *et al.* *William’s Obstetrics*. 20th edition (Stanford CT Appleton and Lange, 1997), pp. 765–7.
- [8] Benirschke K, Kaufman P. *Pathology of the Human Placenta*. 4th edition (New York, Springer, 2000), pp. 778–85.
- [9] Barabási AL, Stanley HE. *Fractal Concepts in Surface Growth* (Cambridge University Press, Cambridge, England, 1995).
- [10] Teague MR. Image analysis via the general theory of moments. *J Opt Soc Am* **70**(8): 920–30 (1980).
- [11] Prokop RJ, Reeves AP. A survey of moment-based techniques for unoccluded object representation and recognition. *CVGIP: Graphic Models and Image Processing* **54**(5): 438–60 (1992).

- [12] Salafia CM, Maas E, Thorp JM, Eucker B, Pezzullo JC, Savitz DA. Measures of placental growth in relation to birth weight and gestational age. *Am J Epidemiol* **162**(10): 991–8 (2005).
- [13] McDonald S, Best C, Lam K. The recurrence risk of severe de novo preeclampsia in singleton pregnancies: a population-based cohort. *BJOG* **116**(12): 1578-1584 (2009).
- [14] Iams JD, Berghella V. Care for women with prior preterm birth. *Am J Obstet Gynecol* **203**(2): 89–100 (2010).
- [15] Kinzler WL, Kaminsky L. Fetal growth restriction and subsequent pregnancy risks. *Semin Perinatol* **31**(3): 126–34 (2007).
- [16] Reddy UM. Prediction and prevention of recurrent stillbirth. *Obstet Gynecol* **110**(5): 1151–64 (2007).
- [17] Flint S, Gibb DM. Recurrent second trimester miscarriage. *Curr Opin Obstet Gynecol* **8**(6): 449–53 (1996).
- [18] Regan L, Rai R. Epidemiology and the medical causes of miscarriage. *Baillieres Best Pract Res Clin Obstet Gynaecol* **14**(5): 839–54 (2000).
- [19] Yampolsky M, Salafia CM, Shlakhter O, Haas D, Eucker B, and Thorp J. Modeling the variability of shapes of a human placenta. *Placenta* **29**(9): 790–7 (2008).
- [20] Feller, W. *An Introduction to Probability Theory and Its Applications*. Vol. 1. 3rd edition. (New York, Wiley, 1968).
- [21] Limpert E, Stahel WA, Abbt M. Log-normal distributions across the sciences: Keys and clues. *BioScience* **51**(5): 341–52 (2001).
- [22] Tsallis C. Lévy distributions. *Phys. World* **10**(7): 42–5 (1997).
- [23] Kaufman JS, Dole N, Savitz DA, Herring, AH. Modeling community-level effects on preterm birth. *Ann Epidemiol* **13**(5): 377–84 (2003).
- [24] Kliman HJ. Umbilical cord, in *Encyclopedia of Reproduction*, E. Knobil and J. Neill, eds., vol. 4, (Academic Press, New York, NY, USA, 1998), pp. 585596.